Real-time spectroelectrochemical monitoring of the diazonium electrografting

Laure Pichereau, Christelle Gautier, Tony Breton

Real-time Spectroelectrochemical Monitoring of the Diazonium Electrografting

Laure Pichereau, Christelle Gautier* and Tony Breton*

Univ Angers, CNRS, MOLTECH-ANJOU, SFR MATRIX, 49000, Angers, France.

Abstract

This work reports the first in-situ and real-time resolved spectroelectrochemical monitoring of a diazonium electrografting. Exploiting the 4-nitrobenzene diazonium salt reduction, we provide a spectral characterization of the adsorption kinetics and confirm the control of the layer growth by using dissolved atmospheric dioxygen as a redox mediator. Gravimetric data were used to rationalize the absorption results and confirm the accuracy of the coupled technique. By comparing the deposition on gold and carbon substrates, the spectroelectrochemical measurements highlighted the impact of the underlying material on the spectral behavior of the organic layer and suggested the existence of an unexpected interface continuum.

Introduction

A substantive work has been undertaken in recent years to develop methods for the functionalization of a wide variety of substrates in view of preparing 2D nanomaterials which exhibit both a high activity and a good sustainability. Among all electrografting techniques available,[1–4] special efforts have focused on the reduction of diazonium salts likely thanks to the ease of the technique implementation[5–7] and the possibilities offered for "on-surface" chemistry.[8,9] The strength of the "diazonium approach" also lies on the efficient and quick grafting of the aryl radicals electrochemically produced.[10–13] However, such mechanism leads, in the vast majority of cases, to an uncontrolled polymerization, and *in fine*, to disorganized organic structures.[14–19] Efforts have been undertaken to work on the film thickness limitation and have led to the development of several efficient control strategies by playing with the steric hindrance of the diazonium structure[20–24] or limiting the local concentration of the reactive radical at the substrate-solution interface.[24–27] However, despite few works focused on local imaging characterization,[28–31] the detailed structure, and thus the physical/chemical properties of the organic layers, remains largely unknown. In this article, we propose to carry out an *in-situ* monitoring of the grafting of 4-nitrobenzene diazonium by absorption spectroelectrochemistry (A-SEC). This highly sensitive home-made measuring bench provides a new perspective to follow the grafting kinetic and get information on the organic layer structuration and its interactions with the supporting substrate.[32] Deposition conditions were varied on carbon and gold to extract new data about the layer structuration.

Results and discussion

The 4-nitrobenzene diazonium (4-NBD) has been extensively used as a benchmark to characterize the grafting behaviour of diazonium salts on surface.[33–36] The electrochemically assisted process is described as a single electron reduction, followed by the spontaneous covalent coupling of the radical generated with the surface (Scheme 1). The high reactivity of the radical intermediate usually leads to the obtention of polyphenylene structures of few

nanometers thickness. Those films have been extensively characterized using various techniques including IR, Raman, XPS and TOF-SIMS but the detailed structure is still poorly understood.

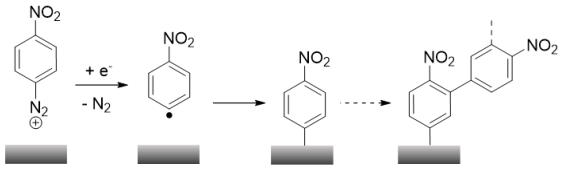

Scheme 1. Electrografting mechanism of the nitrobenzene diazonium on glassy carbon

In order to get informative data on the layer composition and obtain reliable value for the deposition kinetics, the grafting of 4-NBD has been in-situ monitored using a highly sensitive spectroelectrochemical bench. The monitoring was recorded in reflexion mode on glassy carbon electrodes during two voltammetric cycles (between +0.4 and -0.8 V) in the 400-900 nm domain. A classical current-voltage curve was observed, showing two reduction peaks on the first cycle (+0.16 V and -0.14 V) for the aryl radical formation (Figure S2). The presence of two peaks has been previously discussed and was attributed to catalyzed and uncatalyzed reduction processes on the carbon substrate.[37] The strong passivation behavior evidenced for the second and subsequent cycles is consistent with the insulating layer formation.[5]

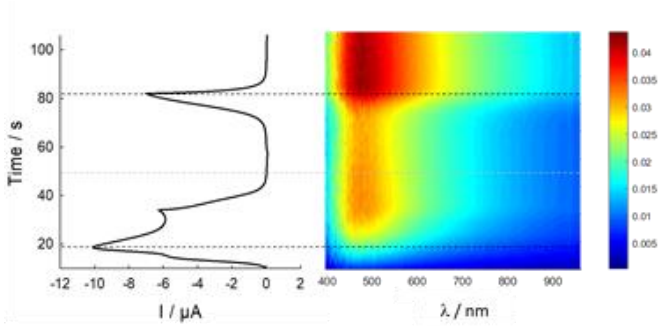

Figure 1. A-SEC over cyclic voltammograms (2 cycles) recorded on GC electrode in the presence of 1 mM 4-NDB between +0.4 and -0.8 V.

The voltabsorptogram presented in Figure 1 shows the variation of the ΔAbs value as function of the applied potential and the unfolded voltammogram versus time is superimposed to the figure for a better comprehension. An increase of ΔAbs is observed at the first diazonium reduction peak (i.e. +0.2 V, 4s) and a large absorption band centered at 470 nm is visible. Δabs values were extracted from this voltabsorptogram at 470 nm (i.e. the maximum values) and are presented in Figure 2. The two grafting steps, corresponding to the first and second negative sweeps, are clearly visible. A steady state value is reached during the first reverse scan (between 30 and 65 s) and a second increase, starting at more negative potential (i.e. -0.5 V, 65 s) is observed during the second cycle. This potential shift is attributed to the barrier effect of the layer formed, which makes more difficult the diazonium electroreduction. The persistence of the signal during the positive sweeps, for which no diazonium reduction occurs, is consistent with the presence of an organic layer on the carbon surface. In the case of species produced in solution at the interface, the semi-infinite diffusion conditions would have provoked a rapid decrease of ΔAbs.

In the aim of rationalizing the relative absorption measurements and linking the data to adsorbed material amount, an *in-situ* monitoring of the grafting was performed using a quartz crystal microbalance. A carbon-coated resonator was functionalized following the 2-cycle potential program described above. The results are presented in Figure 2 in parallel with the Δabs evolution.

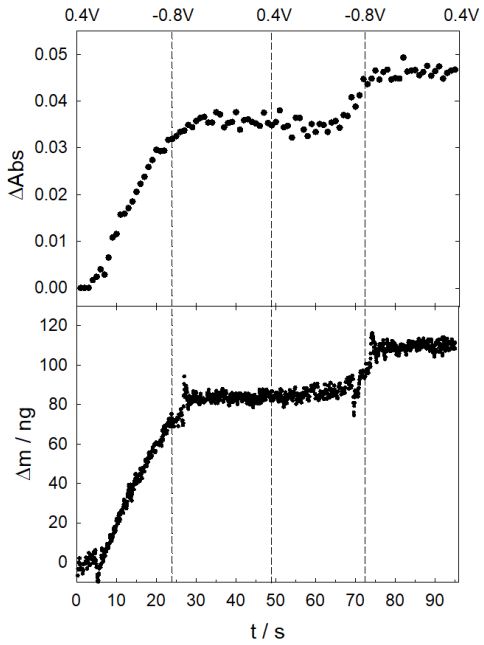

Figure 2. (a) ΔAbs = f(t) at 470 nm recorded on GC electrode in the presence of 1 mM of 4-NDB between +0.4 and -0.8 V for 2 cycles. (b) Mass variation recorded on a 0.5 cm^2 carbon-coated quartz in the presence of 1 mM of 4-NDB between +0.4 and -0.8 V for 2 cycles.

The mass increase is clearly divided in two sequences, corresponding to the two successive reduction waves, respectively starting at +0.2V for the first cycle and -0.6V for the second one. As expected, stable values were obtained for low reduction current, confirming that no grafting occurs without a sufficient driving force generating aryl radicals. A striking comparison of the ΔAbs and mass variation (Δm) can be observed on Figure 2. From the plotted data, the correlation between Δm and ΔAbs is obvious and a linear relationship was obtained (see Figure S2). This correlation means that the spectroscopic signal is proportional to the nitrophenyl surface concentration and thus that all the immobilized species are probed by the light beam. This full response is not surprising since the highest surface concentration value calculated from the gravimetric data is of the order of 1.8×10^{-9} $mol.cm^{-2}$ after a 2-cycle grafting, which corresponds to a thickness of about 4 nanometers according to our previous works.[16] A correlation coefficient of 27 a.u. .$\mu mol^{-1}cm^2$ can be calculated from the extracted data of the Figure S2, considering a film only constituted by nitrophenyl moieties (a.u. being the unit for the absorbance variation ΔAbs).

In view of what is observed for the UV-visible absorption spectrum of the 4-nitrobenzene (i.e. a narrow band centered at 270 nm),[38] the absorption peak observed in Figure 1 (i.e. broad band centered at 470 nm) cannot be attributed to single unconjugated nitrophenyl moieties and more likely corresponds to structures with extended electronic delocalization. A similar broadening was first reported by McCreery *et coll.,*[39,40] and more recently by DiLabio *et coll.,*[41] for nitroazobenzene layers prepared from diazonium reduction on optically transparent carbon pyrolyzed photoresist film. This effect was attributed to intermolecular interactions and/or delocalization with the carbon substrate. The 200 nm redshift reinforces this assumption and is consistent with the existence of strong interaction phenomena.

In order to extract more informative data, a series of chronoamperometric electroreductions of 4-NBD was carried out at fixed potentials using the following potential-time program: 30 s at +0.5 V, 15 min at E_{Red}, 5 min at +0.5 V. This protocol allows to avoid undesired grafting that could occur for intermediate potentials since no diazonium reduction is possible at +0.5 V. Spectroelectrochemical data were recorded for E_{Red} ranging from -0.2 V to -0.9 V. At a potential of -0.2 V (Figure S3), a ΔAbs increase was observed on the whole spectral range, with a maximum located

at 465 nm, similarly to what was obtained for the voltammetric grafting. The same behavior was observed at -0.4 V (Figure 3) but was characterized by a higher ΔAbs values (i.e. 0.027 versus 0.013 at -0.2 V at the end of the 15 min grafting step). Those results, consistent with the formation of extended layers, can be explained by a more effective grafting at lower potential as the electrochemical driving force leads to higher production of aryl radicals. This interpretation is corroborated by the surface concentration values calculated from cyclic voltammograms recorded on the obtained layers in KOH 0.1M and presented on the Figure S4, (i.e. 1.59×10^{-9} mol.cm^{-2} at -0.2 V, and 2.14×10^{-9} mol.cm^{-2} at -0.4 V). Interestingly, for a grafting potential of -0.9 V, the spectrum is characterized by a constant and narrow absorption band centered at 450 nm, and ΔAbs returns close to its original value when the potential is shifted to +0.5 V. Such observation is consistent with the production of reduced species in solution at the substrate solution interface only followed by a near-monolayer grafting, what is confirmed by a very low surface coverage value of 4.5×10^{-10} mol.cm^{-2} (Cf. Figure S4). The drop of the surface coverage has recently been observed for the grafting when low reduction potentials are applied under atmospheric conditions.[27] It was postulated that reduced atmospheric dioxygen species were responsible for this phenomenon by playing the role of a redox cross inhibitor in the diffusion layer, as already demonstrated for other reducible species.[26,42] The spectroelectrochemical data recorded at –0.6 V clearly show the transition between a controlled grafting regime to a non-controlled one, probably as atmospheric dioxygen is consumed in the cell. Current-time curves recorded during the spectroelectrochemical measurements are presented on Figure S5a. The rapid passivation at -0.4 V and the absence of passivation at -0.9 V are highly consistent with the existence of a multilayer grafting mode and a controlled grafting regime respectively. The transition between constant current and passivation observed at -0.6 V well corroborates the A-SEC data.

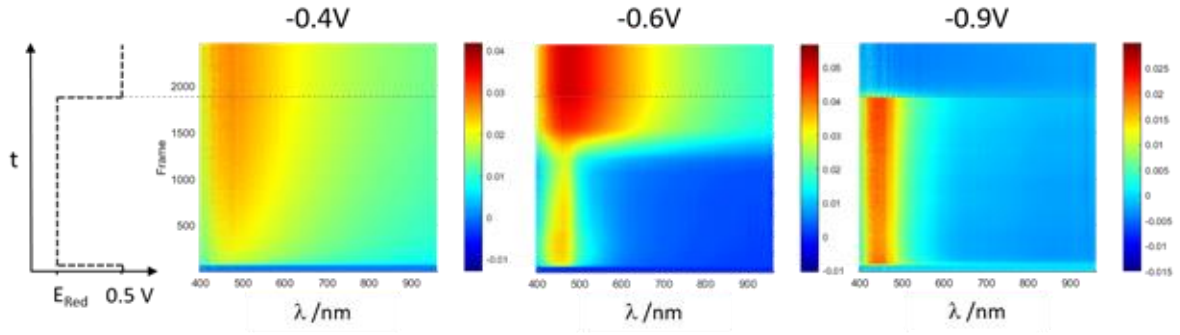

Figure 3. A-SEC over chronoamperometric experiments recorded on GC in the presence of 1 mM 4-NBD in atmospheric conditions for E_{Red} = -0.4, -0.6, and -0.9 V. Potential program: 30 s at +0.5 V, 15 min at E_{Red}, 5 min at +0.5 V.

To confirm the impact of dissolved oxygen on the spectroelectrochemical measurements, a series of chronoamperometric grafting experiments was carried out under inert atmosphere on the same potential range (Figure 4). As obtained under atmospheric conditions at low driving force (i.e. -0.4 V), a broad absorption band was observed on the whole spectral range whatever the potential used. This result corroborates the electrochemical analysis and confirms that in absence of oxygen the grafting efficiency is only governed by the electrochemical driving force. A close examination at the spectra shows that the ΔAbs maximum is only slightly redshifted for the highest driving forces (from 465 nm at -0.2 V to 480 nm at -0.9 V) (see Figure S6 for a A-SEC cut after 8 min at E_{Red}). This observation demonstrates that the thickness, which is linked to the deposited material amount, only has a weak impact on absorption maximum value, and consequently that no strong electronic coupling rises from the multilayer formation. This result is highly consistent with the work reported by McCreery *et coll*. on nitroazobenzene and fluorene, in which the molecular film was considered as a series of weakly interacting organic moieties.[43]

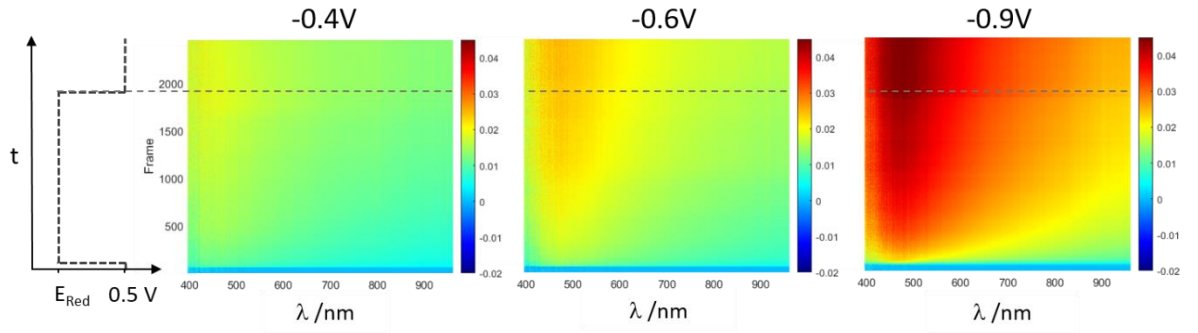

Figure 4. A-SEC over chronoamperometric experiments recorded on GC electrode in the presence of 1 mM 4-NBD under inert atmosphere for E_{Red} = -0.4, -0.6, and -0.9 V. Potential program: 30 s at +0.5 V, 15 min at E_{Red}, 5 min at +0.5 V.

When comparing the absorption spectra obtained under atmospheric and inert conditions, a difference of shape in the signal profile is observable. The superimposition of the normalized data recorded at the end of the grafting step at a potential of -0.6V is presented in Figure S7 for both deposition conditions. The wavelength of the Δabs maximum is substantially the same (i.e. around 470 nm) but the absorption wave appears broader in the case of the grafting carried out under inert atmosphere, with an extension of the absorption over the low energies. In order to determine to what extend the composition of the film is involved in the broadening of the signal, X-ray Photoelectron spectroscopy measurements on films prepared at -0.4 and -0.9 V, in atmospheric and inert conditions, were undertaken. Core level spectra of the N1s region show two main components at 406 and 399.5 eV, respectively attributed to nitro groups and azo functions, previously evidenced on those types of films (Figure S8).[16,44] By comparing the spectra recorded at -0.9 V in both conditions, the grafting control in the presence of dissolved oxygen is clearly evidenced. Indeed, the $N1s_{406}$ atomic percentage is divided by a factor 4 (i.e. from 4.96 to 1.32%) when dioxygen is added in the deposition solution. This drop is very consistent with the surface concentrations extracted from the voltammetric studies (i.e. 2.2×10^{-9} mol.cm^{-2} at -0.4 V and 0.5×10^{-10} mol.cm^{-2} at -0.9 V, see Figure S4). From the $N1s_{400}$/$N1s_{406}$ ratios, the proportion of nitrophenyl groups attached *via* an azo link can be calculated, taking into account 2 reduced nitrogen atoms ($N1s_{400}$) per nitrophenyl function ($N1s_{406}$). At -0.4 V, this proportion is about 15% for the layer prepared under atmospheric conditions and increases to 38% in the absence of oxygen. Similarly, at -0.9 V, this proportion increases from 28 to 57%. The origin of the azo concentration dependence upon the grafting conditions is not explained at the moment but the rise of this concentration inside the film could be responsible for an extension of the electron delocalization, and consequently for the broadening of the absorption wave.

To avoid misinterpretation and generalize our findings, a similar *in-situ* monitoring approach of the grafting was carried out using 1-anthraquinone diazonium salt (1-AQD) instead of 4-NBD. This diazonium salt is known to undergo an efficient grafting and its redox responsive quinone group allows an accurate quantification of the surface concentration using cyclic voltammetry. The series of A-SEC measurements presented on Figure S9 shows the spectroscopic signal recorded under atmospheric and inert conditions at -0.4, -0.6 and -0.9 V. Under atmospheric conditions, the absorption signal at -0.4 V is similar to the one recorded for the 4-NDB grafting, consisting in a broad band centered at 470 nm with an increase of Δabs on the whole spectral range. At a potential of -0.9 V, a narrower absorption band slightly blue shifted (i.e. 445 nm) was observed during the reduction potential imposition, before dropping for the last potential step at +0.5 V. Similarly to what was observed in the case of the 4-NBD electroreduction, this behavior is consistent with the production of a reduced specie in solution, coupled to only a weak grafting, as attested by the final Δabs values (around 1×10^{-2} u.a.). The anthraquinone surface concentrations of the modified carbon electrodes calculated from the voltammetric studies in KOH confirmed the A-SEC values,

showing a drop from 10.5 × 10^{-10} mol.cm^{-2} at -0.4 V to 1 × 10^{-10} mol.cm^{-2} at -0.9 V (see Figure S10). In the absence of oxygen, the absorption intensity increases with the driving force, as observed for the 4-NBD electroreduction. With respect to global spectral behaviour, the same broadening phenomenon is observed when the graftings are carried out under oxygen-free conditions, highlighting a difference in the layer structuration/composition. Finally, it is noteworthy to note that very similar absorption maxima and band shapes are obtained for both grafted moieties despite clearly different UV-vis spectra under their free form (i.e. one band centered at 270 nm for the 4-nitrophenyl group[38] and splitted band at 250 nm with a weaker one at 324 nm for anthraquinone[45]).

In order to investigate the role of the substrate on the spectral behaviour, a series of electrochemical graftings was undertaken on polycrystaline gold under atmospheric conditions using the same protocol at -0.4, -0.6 and -0.9 V (Figure 5). Gold is known to undergo efficient diazonium grafting involving quasi-covalent Au-N or Au-C links.[15,46] For low driving force (i.e. -0.4 V), an absorption band centered at 485 nm was observed immediately after the potential imposition. The signal increases with time and holds at a constant value when the potential is switched to +0.5 V, what is consistent with a progressive grafting on the gold surface during the negative potential step. Even if the absorption maxima are quite similar (i.e. around 480 nm), the narrow shape of the absorption band totally differs from that obtained on carbon.

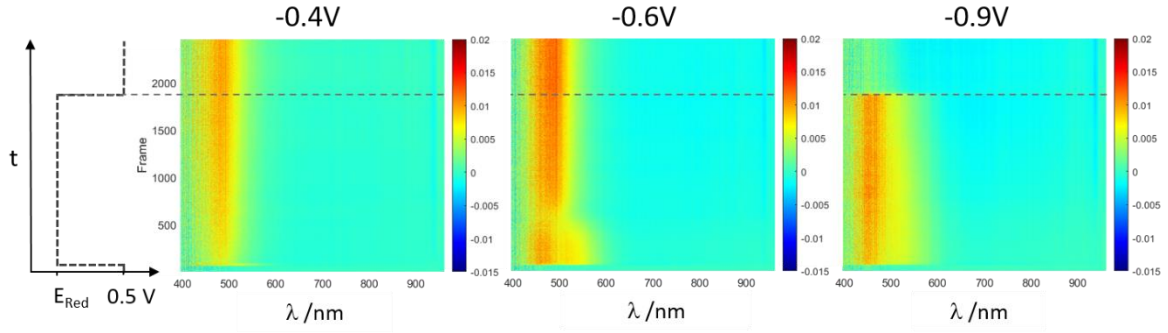

Figure 5. A-SEC over chronoamperometric experiments recorded on polycrystalline gold electrode in the presence of 1 mM 4-NBD in atmospheric conditions for E_{Red} = -0.4, -0.6, and -0.9 V. Potential program: 30 s at +0.5 V, 15 min at E_{Red}, 5 min at +0.5 V.

This surprising result highlights the preponderant role of the substrate on the spectroscopic response. Assuming a similar multilayer structuration of the organic layer on both conductive materials, the broadening observed on carbon appears linked to an electronic interaction at the substrate-film interface. Further work is necessary to characterize this type of interaction but this finding is the strong evidence of a material continuum between the carbon substrate and the organic layer. This spectral behavior also supports the work of De Feyter *et al*. who recently show that a structural change of the carbon surface occurs during the grafting.[29]

For high driving force (i.e. -0.9 V), the voltabsorptogram is very similar to that recorded on carbon, consistent with the production of species (absorption maximum at 455 nm) which does not undergo subsequent grafting on the surface (disappearance of the signal after positive switch of the potential). An interesting point is that the slight redshift observed between the ungrafted and grafted species is similar to the one determined for the carbon substrate, likely because of a similar slight electronic delocalization phenomenon. Moreover, as observed on carbon substrate, electroreduction for intermediate driving force (i.e. -0.6 V) let appear a change in the absorption maximum after 380 s, consistent with the transition between uncontrolled and controlled grafting regime. The current-time curves presented in Figure S5b corroborate this observation by highlighting the progressive passivation of the gold electrode within the 400 first seconds.

To reinforce the idea that electronic delocalization existing between the substrate and the organic moieties is mainly responsible for the extended absorption spectra, A-SEC *in situ* monitoring of the 1-AQD grafting at -0.4 V was carried

out on gold and compared with data obtained on glassy carbon (Figure 6). In both cases the persistent absorption signal after the reduction potential step is consistent with a sustainable grafting on the surface. The absorption maximum is around 480 nm on both substrates but the pronounced broadening evidenced on carbon is absent for the modified gold. Those data well corroborate those obtained for the nitrophenyl grafting and confirm that, first, the structure of the benzene diazonium has only a poor impact on the spectrum, and second, the substrate plays a major role on the signal broadening.

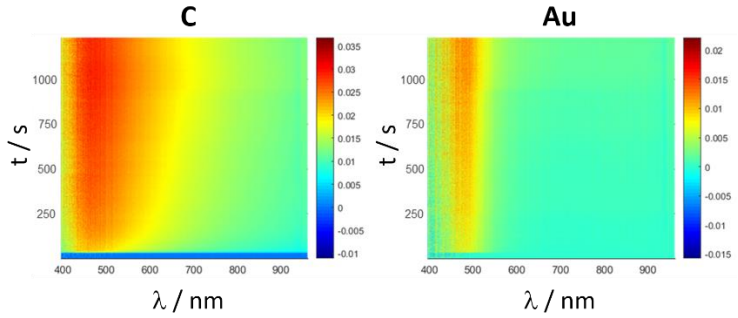

Figure 6. A-SEC over chronoamperometric experiments recorded on glassy carbon (left) and polycrystalline gold (right) electrode in the presence of 1 mM 1-AQD in atmospheric conditions for E_{Red} = -0.4 V. Potential program: 30 s at +0.5 V, 15 min at E_{Red} = -0.4 V, 5 min at +0.5 V.

Efforts have been undertaken to get information on the layer structure thanks to the spectral signature centered around 470 nm on GC. As previously mentioned, the broadening of the signal observed for grafted molecules would mainly come from interactions with the substrate. Considering the grafting mechanism proposed by Pinson *et coll.*[14,44] and the few works focused on the film composition,[11,46–48] the layer should be composed of nitrophenyl oligomers incorporating a variable proportion of azo links coming from the radical attack of non dediazoniated ions. In the field of azo dyes, the substitution of a ring by N-disubstituted groups is known to drive to absorption bands around 500 nm but the existence of such groups is unlikely in the film coming from nitrobenzene diazonium salt.[49,50] UV-Vis simulations of various sizes of oligomers designed to mimic the layer structure were undertaken using Gaussian Software (see Figure S11 for the structures and Table S1 for calculation report and electronic distributions). The carbon substrate was replaced by a methyl group in order to simulate a moderate electron donating behavior. From the obtained spectra, it appears clear that an absorption signal in the visible window cannot be linked to poly-nitrophenyl structures, which all absorb in the UV range whatever the oligomer length is. However, a significant redshift of the absorption spectrum can be obtained by combining azo functions to nitrobenzene groups (i.e. λ_{max} = 340 nm for compound D), due to the rise of an extended electronic conjugation. More precisely, computational details presented in Table S1 showed a decrease of the azo doublet electron density for the benefit of the nitro groups. This redshift remains however not sufficient to fit with the spectral measurements discussed above and would likely be due to a combination of the chemical structure of the organic film with interaction with the substrate.

Experimental

4-nitrobenzenediazonium tetrafluoroborate was used as received from Aldrich. 1-anthaquinone diazonium tetrafluoroborate was prepared from the corresponding aniline according to standard procedures.[10] Glassy carbon (GC) and polycrystalline gold electrodes were obtained from Bioanalytical Systems Inc. (Model MF-2012; diameter 3 mm and 1.6 mm respectively). All potentials were reported versus $Ag/AgNO_3$ (10 mM) reference electrode. CG and gold electrode surfaces were cleaned by polishing with Buehler 1 and 0.04 μm alumina slurry. After each

polishing step the electrode was washed with nanopure water (18.2 MΩ cm) under sonication. Prior and after each electrochemical derivatization, the electrode was sonicated in acetonitrile for 1 minute.

Time-resolved spectroelectrochemistry measurements were performed by using an already-described home-made cell.[51] A scheme of the setup is presented in Figure S12. Electrochemical measurements were carried out by using a platinum wire counter electrode and a $Ag/AgNO_3$ (10 mM) reference electrode with a Biologic SP-150 potentiostat driven by EC-Lab software. Experiments were recorded in HPLC-grade acetonitrile with tetrabutylammonium hexafluorophosphate (Bu_4NPF_6, electrochemical grade, Aldrich) as the supporting electrolyte. Spectrophotometric measurements were carried out in direct reflexing mode on the working electrode (glassy carbon or gold) with a home-made bench composed of different Princeton Instruments modules (light sources, fibers, monochromators, spectroscopy camera, and software). The connection between the light source, the cell, and the spectrophotometer is ensured through a "Y-shaped" optical fiber bundle: 18 fibers guide the light to the cell and 19 fibers collect the reflected light from the cell to visible (400–900 nm/maximum acquisition frequency 2 MHz) CCD detector. The sensitivity of the spectroscopic measurement (<3 electrons at 100 kHz and <13 electrons at 2 MHz between 400 and 900 nm) allows a spectroelectrochemistry experiment to be performed under the usual conditions of electrochemistry. For each data set, the reference intensity (I_{ref}) was obtained by averaging the intensity of the first 10 measured frames. Consequently, absorbance variations ($\Delta Abs = - \log_{10}(I/I_{ref})$) and not absorbance values were monitored.

Electrochemical quartz crystal microbalance (EQCM) measurements were performed with a QCA922 (Seiko-EG&G, Princeton Applied Research) equipped with a carbon-coated quartz crystal (Biologic SE-9C-M) in a closed cell (Biologic SE-CL3 model) and coupled to a SP300 Biologic potentiostat, both driven by EC-Lab software. The cell was used in vertical set up equipped with a platinum wire as counter electrode and a $Ag/AgNO_3$ reference electrode. EQCM experiments were carried out to monitor the mass change of the electrode during the electrochemical reduction of the diazonium cation under the electrochemical modification conditions described above.

XPS data were collected using a Kratos Axis Ultra spectrometer on modified GC sheets (Goodfellow, model VC 551). Films were deposited in the presence of 1 mM diazonium at a controlled potential of -0.4 or -0.9 V for 15 min. The X-ray source was monochromated Al Kα working at 1486.6 eV. Spectra were accumulated at a take off angle of 90°, using a spot size of 0.7×0.3 mm2 at a pressure of less than 10^{-8} mbar. High resolution scans (N 1s) were carried out with 0.1 eV step size and pass energy 20 eV. All spectra were calibrated taking C 1s as a reference binding energy of 284.5 eV (graphitic carbon component of the glassy carbon substrates), without internal standard. XPS spectra were analyzed with the curve fitting program CASA XPS and involved background subtraction using Shirley and a subsequent pseudo-Voigt function mixing Gaussian-Lorentzian functions. Atomic ratios of the surfaces were calculated from core level spectra normal area divided by number of scans and the element sensitivity factor (1.78 for N 1s and 1.00 for C 1s).

For all calculations, the Gaussian 09 software (revision D.01) has been used.[52] All ground states in gas phase have been optimized by a DFT approach with the PBE1PBE hybrid functional and the 6–311+G(2d,2p) basis set.[53] A Time Dependent DFT method has been employed to compute the first 15 excited singlet states with the same level of theory. The simulated UV-visible absorption spectra have been obtained by Gaussian broadening of the calculated transition energies (FWHM of 3000 cm^{-1}). Atomic charge mapping has been obtained by Hirshfeld population analysis taking into account interatomic electrostatic interactions. The full molecular reports, molecular orbitals, electron density differences pictures and calculated spectra have been automatically generated by a homemade Python program, quchemreport, based on cclib.[54,55]

Conclusions

The first *in-situ* and real-time absorption spectroelectrochemical monitoring of a diazonium electrografting highlighted the potential of this coupled technique to get access to kinetic and fundamental information on the chemical structuration of attached layers. Applied to the 4-nitrobenzene diazonium electrografting, a good correlation between gravimetric data obtained from quartz crystal microbalance experiments and absorption values was evidenced. A singular broadening of the spectral signature was observed over the whole visible range for the adsorbed species, as well as an unexpected redshift of the signal. The strong electronic delocalization exhibited by the carbon-supported layer compared to the gold-supported one forces us to reconsider the functionalized carbon as a new interface, exhibiting a singular electronic behavior. Extension of the study to the 1-anthraquinone electrografting corroborated the results and proved that the highlighted phenomena are not structure-dependent. The role of activated atmospheric dioxygen as a redox inhibitor for the grafting was confirmed by the A-SEC measurements and the spectral transition between controlled regime and multilayer deposition was visualized. Under controlled deposition regime, the A-SEC data showed the presence a species, characterized by a narrow absorption band around 450 nm. Efforts will be made to identify the corresponding structure, which could be a key intermediate for the diazonium electrografting.

Electronic Supplementary Information (ESI) available: cyclic voltammograms, voltabsorptograms, calculated surface coverages, correlation between mass and absorbance, current-time curves, 2D-absorption spectra, normalized absorption spectra, XPS core level spectra, absorption spectroelectrochemistry setup, simulated UV-Vis spectra and UV-Vis calculation report. See DOI: 10.1039/x0xx00000x

Author Contributions

Laure Pichereau conducted the investigations and the validation of the results. Christelle Gautier and Tony Breton both conceptualized the research ideas, supervised the project and wrote the manuscript. The research methodology was a common work of the three authors.

Conflicts of interest

There are no conflicts to declare.

Acknowledgements

This work was supported by the "Centre National de la Recherche Scientifique" (CNRS France), the "Agence Nationale de la Recherche" (ANR France), and the "Région des Pays de la Loire" (France). The authors thank Dr. Thomas Cauchy for his assistance in the UV-Vis computational work.

Notes and references

1 D. Belanger and J. Pinson, *Chemical Society Reviews*, 2011, **40**, 3995–4048.
2 J. J. Gooding and S. Ciampi, *Chem. Soc. Rev.*, 2011, **40**, 2704.

3 J. Pinson, *Current Opinion in Electrochemistry*, 2020, 5.
4 D. Wang, M. K. Khan and M. G. Moloney, *Tetrahedron Letters*, 2020, **61**, 151672.
5 J. Pinson and F. Podvorica, *Chem. Soc. Rev.*, 2005, **34**, 429.
6 S. Mahouche-Chergui, S. Gam-Derouich, C. Mangeney and M. M. Chehimi, *Chem. Soc. Rev.*, 2011, **40**, 4143–4166.
7 D. Hetemi, V. Noël and J. Pinson, *Biosensors*, , DOI:10.3390/bios10010004.
8 C. Gautier, I. López and T. Breton, *Mater. Adv.*, 2021, **2**, 2773–2810.
9 T. Wu, C. M. Fitchett, P. A. Brooksby and A. J. Downard, *ACS Appl. Mater. Interfaces*, 2021, **13**, 11545–11570.
10 P. Allongue, M. Delamar, B. Desbat, O. Fagebaume, R. Hitmi, J. Pinson and J.-M. Savéant, *Journal of the American Chemical Society*, 1997, **119**, 201–207.
11 C. Saby, B. Ortiz, G. Y. Champagne and D. Bélanger, *Langmuir*, 1997, **13**, 6805–6813.
12 S. Bouden, J. Pinson and C. Vautrin-Ul, *Electrochemistry Communications*, 2017, **81**, 120–123.
13 S. Phal, K. Shimizu, D. Mwanza, P. Mashazi, A. Shchukarev and S. Tesfalidet, 2020, 12.
14 A. Adenier, C. Combellas, F. Kanoufi, J. Pinson and F. I. Podvorica, *Chem. Mater.*, 2006, **18**, 2021–2029.
15 A. Laforgue, T. Addou and D. Bélanger, *Langmuir*, 2005, **21**, 6855–6865.
16 T. Menanteau, E. Levillain, A. J. Downard and T. Breton, *Phys. Chem. Chem. Phys.*, 2015, **17**, 13137–13142.
17 T. Menanteau, E. Levillain and T. Breton, *Chem. Mater.*, 2013, **25**, 2905–2909.
18 B. M. Simons, J. Lehr, D. J. Garrett and A. J. Downard, *Langmuir*, 2014, **30**, 4989–4996.
19 K. Tahara, Y. Kubo, B. Lindner, S. Hashimoto, S. Hirose, A. Brown, B. Hirsch, L. Daukiya, S. De Feyter and Y. Tobe, *Langmuir*, 2019, **35**, 2089–2098.
20 C. Combellas, F. Kanoufi, J. Pinson and F. I. Podvorica, *J. Am. Chem. Soc.*, 2008, **130**, 8576–8577.
21 K. Malmos, J. Iruthayaraj, S. U. Pedersen and K. Daasbjerg, *J. Am. Chem. Soc.*, 2009, **131**, 13926–13927.
22 K. Malmos, M. Dong, S. Pillai, P. Kingshott, F. Besenbacher, S. U. Pedersen and K. Daasbjerg, *J. Am. Chem. Soc.*, 2009, **131**, 4928–4936.
23 Y. R. Leroux, H. Fei, J.-M. Noël, C. Roux and P. Hapiot, *Journal of the American Chemical Society*, 2010, **132**, 14039–14041.
24 T. Breton and A. J. Downard, *Australian Journal of Chemistry*, 2017, **70**, 960.
25 O. Fontaine, J. Ghilane, P. Martin, J.-C. Lacroix and H. Randriamahazaka, *Langmuir*, 2010, **26**, 18542–18549.
26 I. López, S. Dabos-Seignon and T. Breton, *Langmuir*, 2019, **35**, 11048–11055.
27 L. Pichereau, I. López, M. Cesbron, S. Dabos-Seignon, C. Gautier and T. Breton, *Chem. Commun.*, 2019, **55**, 455–457.
28 R. Steeno, M. C. Rodríguez González, S. Eyley, W. Thielemans, K. S. Mali and S. De Feyter, *Chem. Mater.*, 2020, **32**, 5246–5255.
29 J. Greenwood, T. H. Phan, Y. Fujita, Z. Li, O. Ivasenko, W. Vanderlinden, H. Van Gorp, W. Frederickx, G. Lu, K. Tahara, Y. Tobe, H. Uji-i, S. F. L. Mertens and S. De Feyter, *ACS Nano*, 2015, **9**, 5520–5535.
30 V. Q. Nguyen, X. Sun, F. Lafolet, J.-F. Audibert, F. Miomandre, G. Lemercier, F. Loiseau and J.-C. Lacroix, *J. Am. Chem. Soc.*, 2016, **138**, 9381–9384.
31 H. Van Gorp, P. Walke, J. Teyssandier, B. E. Hirsch, H. Uji-i, K. Tahara, Y. Tobe, M. Van der Auweraer and S. De Feyter, *J. Phys. Chem. C*, 2020, **124**, 1980–1990.
32 O. Alévêque, C. Gautier and E. Levillain, *Current Opinion in Electrochemistry*, 2019, **15**, 34–41.
33 B. Ortiz, C. Saby, G. Y. Champagne and D. Bélanger, *Journal of Electroanalytical Chemistry*, 1998, **455**, 75–81.
34 J. Lehr, B. E. Williamson and A. J. Downard, *J. Phys. Chem. C*, 2011, **115**, 6629–6634.
35 S. S. C. Yu, E. S. Q. Tan, R. T. Jane and A. J. Downard, *Langmuir*, 2007, **23**, 11074–11082.
36 M. Ceccato, L. T. Nielsen, J. Iruthayaraj, M. Hinge, S. U. Pedersen and K. Daasbjerg, *Langmuir*, 2010, **26**, 10812–10821.
37 L. Lee, P. A. Brooksby, P. Hapiot and A. J. Downard, *Langmuir*, 2016, **32**, 468–476.
38 S. Nagakura, M. Kojima and Y. Maruyama, *Journal of Molecular Spectroscopy*, 1964, **13**, 174–192.
39 H. Tian, A. J. Bergren and R. L. McCreery, *Appl. Spectrosc.*, 2007, **61**, 1246–1253.
40 A. M. Mahmoud, A. J. Bergren and R. L. McCreery, *Anal. Chem.*, 2009, **81**, 6972–6980.
41 C. Van Dyck, A. J. Bergren, V. Mukundan, J. A. Fereiro and G. A. DiLabio, *Phys. Chem. Chem. Phys.*, 2019, **21**, 16762–16770.
42 I. López, M. Cesbron, E. Levillain and T. Breton, *ChemElectroChem*, 2018, **5**, 1197–1202.
43 A. Morteza Najarian and R. L. McCreery, *ACS Nano*, 2017, **11**, 3542–3552.
44 P. Doppelt, G. Hallais, J. Pinson, F. Podvorica and S. Verneyre, *Chem. Mater.*, 2007, **19**, 4570–4575.
45 M. F. Jacobsen, E. E. Ferapontova and K. V. Gothelf, *Org. Biomol. Chem.*, 2009, **7**, 905.
46 A. Mesnage, X. Lefèvre, P. Jégou, G. Deniau and S. Palacin, *Langmuir*, 2012, **28**, 11767–11778.

47 Y.-C. Liu and R. L. McCreery, *J. Am. Chem. Soc.*, 1995, **117**, 11254–11259.
48 P. A. Brooksby and A. J. Downard, *The Journal of Physical Chemistry B*, 2005, **109**, 8791–8798.
49 P. C. Chen, Y. C. Chieh and J. C. Wu, *Journal of Molecular Structure-theochem*, 2005, **715**, 183–189.
50 L. Zhang and J. M. Cole, *Phys. Chem. Chem. Phys.*, 2016, **18**, 19062–19069.
51 O. Alévêque, E. Levillain and L. Sanguinet, *Electrochemistry Communications*, 2015, **51**, 108–112.
52 *M. J. Frisch, G. W. Trucks, H. B. Schlegel, G. E. Scuseria, M. A. Robb, J. R. Cheeseman, G. Scalmani, V. Barone, B. Mennucci, G. A. Petersson, H. Nakatsuji, M. Caricato, X. Li, H. P. Hratchian, A. F. Izmaylov, J. Bloino, G. Zheng, J. L. Sonnenberg, M. Hada, M. Ehara et al., Gaussian ~09 Revision D.01.*
53 C. Adamo and V. Barone, *The Journal of Chemical Physics*, 1999, **110**, 6158–6170.
54 N. M. O'boyle, A. L. Tenderholt and K. M. Langner, *Journal of Computational Chemistry*, 2008, **29**, 839–845.
55 T. Cauchy and B. Da Mota, *University of Angers, 2020*.